3.7.1

Dynamic Kerr effect in a strong uniform AC electric field for interacting polar and polarizable molecules in the mean field approximation

Snehal D. Deshmukh, Pierre-Michel Déjardin, and Yuri P. Kalmykov

Citation: The Journal of Chemical Physics **147**, 094501 (2017); doi: 10.1063/1.4995021
View online: http://dx.doi.org/10.1063/1.4995021
View Table of Contents: http://aip.scitation.org/toc/jcp/147/9
Published by the American Institute of Physics

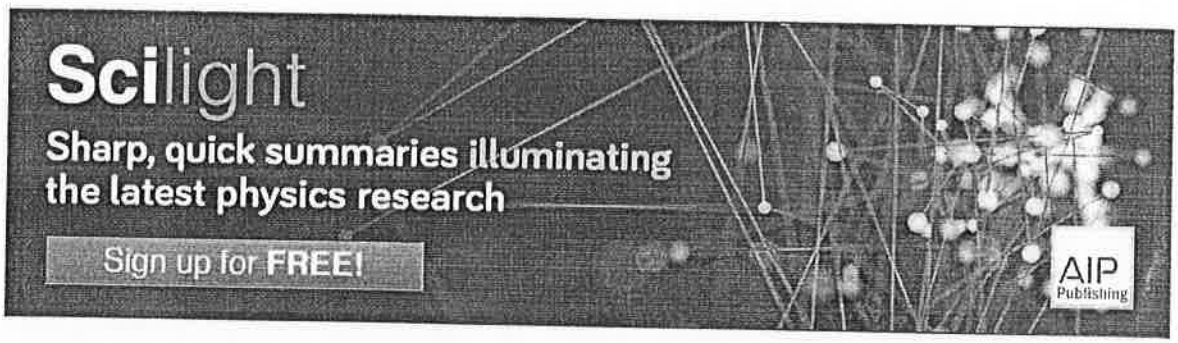

Dynamic Kerr effect in a strong uniform AC electric field for interacting polar and polarizable molecules in the mean field approximation

Snehal D. Deshmukh,[1,2] Pierre-Michel Déjardin,[2] and Yuri P. Kalmykov[2]
[1]*Microwave Research Lab, Department of Physics, Dr. B. A. M. University, Aurangabad, 431004 Maharashtra, India*
[2]*Laboratoire de Mathématiques et Physique (EA 4217), Université de Perpignan Via Domitia, 52 Avenue Paul Alduy, 66860 Perpignan Cedex, France*

(Received 10 July 2017; accepted 15 August 2017; published online 5 September 2017)

Analytical formulas for the electric birefringence response of interacting polar and anisotropically polarizable molecules due to a uniform alternating electric field are derived using Berne's forced rotational diffusion model [B. J. Berne, J. Chem. Phys. **62**, 1154 (1975)] in the nonlinear version described by Warchol and Vaughan [J. Chem. Phys. **71**, 502 (1979)]. It is found for noninteracting molecules that the signal consists of a frequency-dependent DC component superimposed on an oscillatory part with a frequency twice that of the AC driving field. However, unlike noninteracting molecules, the AC part strongly deviates from its dilute counterpart. This suggests a possible way of motivating new experimental studies of intermolecular interactions involving electro-optical methods and complementary nonlinear dielectric relaxation experiments. *Published by AIP Publishing.* [http://dx.doi.org/10.1063/1.4995021]

I. INTRODUCTION

Nonlinear dielectric and Kerr effect relaxation in polar fluids springs from the rotational motion of molecules in the presence of externally applied electric fields and thermal agitation.[1–4] Both these effects are treated via nonlinear response theory, which is mathematically much more involved than its linear counterpart, because unlike in the former, no connection between the transient and AC responses exists. This is exemplified via the calculation of the dynamic Kerr effect, where the square field law rectifies the pure sinusoidal electric field yielding a DC frequency-dependent response superposed on which is a dephased second harmonic part.[5,6] The calculation of the birefringence signal is generally undertaken by assuming that intermolecular interactions are negligible, and the first author to make such a calculation was Benoit.[7] This calculation was revisited in the general context of nonlinear dielectric relaxation phenomena by Coffey and Paranjape.[8] The theory developed by all these authors corresponds to a situation where the dipole-dipole interactions have been effectively eliminated by suitable extrapolation of experimental data to infinite dilution,[9] if this extrapolation is possible. Nevertheless, situations exist, where the extrapolation is meaningless, for example, in dense dipolar systems. There the intermolecular interactions cannot be neglected. Then, the calculation of the Kerr effect signal under an AC field becomes very complicated in two respects: (a) because the system has more than one degree of freedom and (b) the field involved in the calculation is the molecular field which differs from the applied field.

In *linear* dielectric relaxation, part (a) of the problem was first addressed by Zwanzig.[10] He set up the multi-dipole Fokker-Planck equation for the distribution function of orientations of the entire dipolar assembly and approximately solved by using perturbation methods. Thus, he was able to demonstrate that dielectric relaxation *formally* consists of an infinite set of microscopic relaxation processes. However, a systematic method of truncating the perturbation series is unknown. Due to this difficulty, Zhou and Bagchi[11] revisited Zwanzig's model and observed exponential decay of the dipole relaxation function via numerical simulation methods. However, a rather different approach to dielectric relaxation was introduced by Berne[12] and Warchol and Vaughan.[13] Their theory commences with a nonlinear Smoluchowski equation from whereby they obtain the dipole correlation function pertaining to dielectric relaxation. This approach was recently extended by Déjardin[14] to magnetic relaxation of single-domain ferromagnetic particles and by Déjardin and Ladieu[15] with the objective of generalizing the nonlinear dielectric response formulas of Coffey and Paranjape[8] to interacting dipolar systems. In particular, by extending the Madden-Kivelson approach[16] to nonlinear response, they demonstrated[15] that the most complete information that can be gathered from experiment is contained in the nonlinear response itself. By contrast, although affected by interactions via relaxation time and dielectric permittivity magnitude, linear response dielectric spectra were on the whole still qualitatively unaffected, in qualitative agreement with experiment.

Thus, the most difficult theoretical part of the *linear* dielectric relaxation problem consists of part (b), i.e., accounting for the dynamics of the internal (or molecular) field. This problem is extremely complicated as this field depends non-trivially on the macroscopic quantity that is desired, i.e., the complex permittivity. A benchmark allowing the subject to progress lies in the work of Nee and Zwanzig[17] who re-derived the Fatuzzo-Mason equation linking the *linear* complex permittivity to the one-sided Fourier transform of the response function by assuming a special type of memory, i.e., dielectric

0021-9606/2017/147(9)/094501/6/$30.00

friction (a concept that was first put forward by Zwanzig). However, shortcomings of this approach were demonstrated by Zhou and Bagchi.[11] In fact, no substantial progress has been made in this direction since. Furthermore, regarding the nonlinear response, the situation is more complicated even on the static level, as in order to obtain an equation for the internal field equivalent to that of Onsager,[18] one has to account for the non-homogeneity of the local field near the boundary of the molecular sphere introduced by Onsager, which then requires the solution of a nonlinear partial differential equation,[19,20] leading to very difficult calculations. In order to circumvent this, homogeneity of the internal field is generally assumed.[19,21] In the normal dielectric saturation effect, this assumption usually causes the mean field theory and experimental data to differ by at most a factor of 2. Thus, the direct deduction of the dipole moment values from static nonlinear dielectric increment measurements will have an error not exceeding 20% of the literature value.[19] Since theoretical predictions concerning nonlinear response can only be qualitative, even fewer *explicit* calculations of the dynamic Kerr effect involving intermolecular interactions exist. We mention in passing the works of Beevers *et al.*[22] and Rosato and Williams[23] who tried to establish a relationship between the rise and decay transients of the Kerr effect signals in terms of certain field-free correlation functions. However, as already alluded to above, in general, the AC Kerr effect cannot be connected to the rise and/or decay transients following the switch on or removal of an external field.

One way of proceeding has been described in Refs. 5 and 6, where (short-range) intermolecular interactions are accounted for via a mean field Maier-Saupe potential (the Debye-Fröhlich model), ultimately leading to the inclusion of Kramers-like[24] thermally activated overbarrier relaxation processes in the Kerr response. This is useful particularly if one calculates the Kerr effect in nematic liquid crystals, or in a first approximation, in a suitable adaptation of the "toy model" proposed by Ladieu *et al.*[25] to the calculation of the Kerr effect in super-cooled liquids. Here, in order to calculate the Kerr effect response, we shall use Berne's approach as used by Déjardin and Ladieu,[15] which will show that although the DC component is qualitatively unaltered by interactions (and hence equivalent to the linear response, as expected), the AC response is, in contrast, drastically affected displaying non-monotonic behavior.

II. DYNAMIC KERR EFFECT IN AN AC ELECTRIC FIELD

We shall consider the nonlinear AC stationary response of an assembly of interacting polar and polarizable particles (electric dipoles) undergoing rotational Brownian motion acted on by a strong external AC field $\mathbf{E}(t) = \mathbf{E}_0 \cos \omega t$. For simplicity, we suppose that $\mathbf{E}_0$ is directed along the Z-axis of the laboratory coordinate system. Following Berne,[12] Warchol and Vaughan[13] and Déjardin and Ladieu,[15] by modeling the orientational relaxation of polar and polarizable molecules via isotropic rotational diffusion, we can write down the *nonlinear* Smoluchowski rotational diffusion equation for the distribution function $W(\vartheta, t)$ of orientations of the dipoles on the unit sphere as

$$\frac{\partial W}{\partial t} = \frac{1}{2\tau_D \sin\vartheta} \frac{\partial}{\partial \vartheta} \left[\sin\vartheta \left(\frac{\partial W}{\partial \vartheta} + \beta W \frac{\partial V_W}{\partial \vartheta} \right) \right], \quad (1)$$

where $\beta = (kT)^{-1}$, k is the Boltzmann's constant, T is the absolute temperature, τ_D is the Debye relaxation time, ϑ is the angle the dipole makes with the Z axis of the laboratory frame, and $V_W(\vartheta, t)$ is the orientational potential energy of a dipole, now given by

$$\beta V_W(\vartheta, t) = -\xi(t) \cos\vartheta - \sigma(t) \cos^2\vartheta + \lambda \langle \cos\vartheta \rangle (t) \cos\vartheta, \quad (2)$$

where $\xi(t) = \xi_0 \cos \omega t$, $\xi_0 = \beta \mu E_0$ is the dimensionless ac field parameter, ω is the frequency of the driving AC field, μ is the dipole moment of a molecule in the liquid phase, $\sigma(t) = \beta \Delta\alpha E_0^2 cos^2(\omega t)/2$, $\Delta\alpha$ is the difference between the principal electric polarizabilities parallel and perpendicular to the symmetry axis, $\lambda = 4\pi\beta\rho_0\mu^2/3$ is the interaction parameter, and ρ_0 is the number of molecules per unit volume. The angular brackets $\langle\rangle$ in Eq. (2) denote an ensemble average over W, viz.,

$$\langle A \rangle (t) = \int_0^\pi A(\vartheta) W(\vartheta, t) \sin\vartheta d\vartheta, \quad (3)$$

where A is an arbitrary function of ϑ. In writing the *nonlinear* Smoluchowski equation, Eq. (1), we have noted that for the axially symmetric potential Eq. (2), the azimuthal angle dependence of the distribution function W may be ignored. In Eq. (2), it is assumed that dipole-induced dipole and induced dipole-induced dipole interactions are negligible in comparison with the permanent dipole-permanent dipole interaction. Furthermore, the results will only be valid in the low-frequency range, $\omega < 10^9$ Hz, as inertial effects are ignored in the model. In detail, the range of the applicability of the model is discussed elsewhere.[13–15]

We solve the rotational diffusion Eq. (1) by expanding $W(\vartheta, t)$ in a generalized Fourier series as

$$W(\vartheta, t) = \sum_{n=0}^{\infty} \left(n + \frac{1}{2} \right) f_n(t) P_n(\cos\vartheta), \quad (4)$$

where $P_n(z)$ is the Legendre polynomial of order n and the Fourier coefficients (relaxation functions) $f_n(t)$ are formally given by

$$f_n(t) = \langle P_n(\cos\vartheta) \rangle (t) = \int_0^\pi P_n(\cos\vartheta) W(\vartheta, t) \sin\vartheta d\vartheta \quad (5)$$

due to the orthogonality property of the P_n, viz.,

$$\int_0^\pi P_n(\cos\vartheta) P_m(\cos\vartheta) \sin\vartheta d\vartheta = \frac{2\delta_{nm}}{2n+1}$$

(δ_{nm} is Kronecker's delta). Substituting Eq. (4) into Eq. (1) and utilizing the properties of the P_n, we have an infinite hierarchy of differential-recurrence equations for the relaxation

functions $f_n(t)$, $n = 1, 2, \ldots$ (in notation of Ref. 15)

$$\frac{2\tau_D}{n(n+1)}\dot{f}_n(t) + \left[1 - \frac{2\sigma(t)}{(2n-1)(2n+3)}\right] f_n(t) = \frac{[\xi(t) - \lambda f_1(t)]}{(2n+1)}\left[f_{n-1}(t) - f_{n+1}(t)\right] + 2\sigma(t) \times \left[\frac{(n-1)}{(2n-1)(2n+1)} f_{n-2}(t) - \frac{(n+2)}{(2n+1)(2n+3)} f_{n+2}(t)\right]. \tag{6}$$

By solving Eq. (6), we shall determine the ac stationary response of the dynamic Kerr effect governed by the birefringence function $K(t)$ defined as[2]

$$K(t) = \frac{2\pi\rho_0}{\bar{n}}\left(\alpha^0_{//} - \alpha^0_{\perp}\right)\langle P_2(\cos\vartheta)\rangle(t). \tag{7}$$

Here $\bar{n}$ is the mean refractive index, $\alpha^0_{//} - \alpha^0_{\perp}$ is the difference between the optical polarizabilities due to the electric field (optical frequency) of the light beam passing through the liquid medium, and $P_2(z)$ is the Legendre polynomial of order 2. Now, Eq. (7) for the birefringence function is valid at frequencies ω well below high frequency resonance absorption peaks. Thus, by solving Eqs. (6), we will have the steady-state birefringence function $K(t) \sim \langle P_2(\cos\vartheta)\rangle(t) = f_2(t)$.

Now, although the applied AC electric field in experiments is high enough ($\geq 10^6$ V/m) to observe nonlinear effects, the energy of the dipole in the field remains sufficiently weak compared to the thermal energy. Thus, we may use perturbation theory to determine the ac stationary response for a weak ac field $\xi(t) = \xi_0 \cos\omega t$ ($\xi_0 << 1$). Since we require the solution of the hierarchy of Eqs. (6) up to quadratic order in the field strength, we may follow Coffey and Paranjape[8] and expand the relaxation functions $f_n(t)$ in powers of the AC field strength up to second order, viz.,

$$f_n(t) = f_n^{(0)} + f_n^{(1)}(t) + f_n^{(2)}(t), \tag{8}$$

where $^{(n)}$ denotes the order in the field strength and so obtain the coupled perturbation equations:

$$n(n+1) f_n^{(0)} = \frac{\lambda n(n+1) f_1^{(0)}}{2n+1}\left[f_{n+1}^{(0)} - f_{n-1}^{(0)}\right], \tag{9}$$

$$\frac{2\tau_D}{n(n+1)}\frac{d}{dt} f_n^{(1)}(t) + f_n^{(1)}(t) = \frac{\xi(t) - \lambda f_1^{(1)}(t)}{2n+1}\left[f_{n-1}^{(0)} - f_{n+1}^{(0)}\right] + \frac{\lambda f_1^{(0)}}{2n+1}\left[f_{n+1}^{(1)}(t) - f_{n-1}^{(1)}(t)\right], \tag{10}$$

$$\frac{2\tau_D}{n(n+1)}\frac{d}{dt} f_n^{(2)}(t) + f_n^{(2)}(t) - \frac{2\sigma(t)}{(2n-1)(2n+3)} f_n^{(0)} = \frac{\xi(t) - \lambda f_1^{(1)}(t)}{2n+1}\left[f_{n-1}^{(1)}(t) - f_{n+1}^{(1)}(t)\right] + \frac{\lambda f_1^{(2)}(t)}{2n+1} \times \left[f_{n+1}^{(0)} - f_{n-1}^{(0)}\right] + \frac{\lambda f_1^{(0)}}{2n+1}\left[f_{n+1}^{(2)}(t) - f_{n-1}^{(2)}(t)\right] + 2\sigma(t) \times \left[\frac{(n-1)}{(2n-1)(2n+1)} f_{n-2}^{(0)} - \frac{(n+2)}{(2n+1)(2n+3)} f_{n+2}^{(0)}\right]. \tag{11}$$

Equations (9) and (10) have already been solved in Ref. 15. The only nonvanishing solutions for $f_n^{(0)}$ and $f_n^{(1)}(t)$ of these equations in the steady-state regime are[15]

$$f_n^{(0)} = \delta_{0n} \tag{12}$$

and

$$f_1^{(1)}(t) = \xi_0\left[\frac{(3+\lambda)\cos\omega t}{(3+\lambda)^2 + 9\omega^2\tau_D^2} + \frac{3\omega\tau_D \sin\omega t}{(3+\lambda)^2 + 9\omega^2\tau_D^2}\right]. \tag{13}$$

Noting Eqs. (12) and (13) and again following closely the method of Coffey and Paranjape,[8] we see that $f_2^{(1)}(t) = 0$. Then by setting $n = 2$ in Eq. (11) and solving the resulting equation by quadratures with the initial condition $f_2^{(2)}(-\infty) = 0$, we have the stationary solution for $f_2^{(2)}(t)$, viz.,

$$f_2^{(2)}(t) = \xi_0^2\left[C(\omega) + \alpha_2'^{(2)}(\omega)\cos 2\omega t + \alpha_2''^{(2)}(\omega)\sin 2\omega t\right]. \tag{14}$$

Here the frequency-dependent coefficients $C(\omega)$, $\alpha_2'^{(2)}(\omega)$, and $\alpha_2''^{(2)}(\omega)$ are

$$C(\omega) = \frac{\gamma}{90} + \frac{3}{10\left((3+\lambda)^2 + 9\omega^2\tau_D^2\right)}, \tag{15}$$

$$\alpha_2'^{(2)}(\omega) = \frac{\gamma}{10(9 + 4\omega^2\tau_D^2)} + \frac{9\left(3(3+\lambda)^2 + (9 + 2\lambda(9+\lambda))\omega^2\tau_D^2 - 18\omega^4\tau_D^4\right)}{10(9 + 4\omega^2\tau_D^2)\left((3+\lambda)^2 + 9\omega^2\tau_D^2\right)^2}, \tag{16}$$

$$\alpha_2''^{(2)}(\omega) = \frac{\gamma\omega\tau_D}{15(9 + 4\omega^2\tau_D^2)} + \frac{9\omega\tau_D\left(45 + 12\lambda - \lambda^2 + 3(15 + 4\lambda)\omega^2\tau_D^2\right)}{10(9 + 4\omega^2\tau_D^2)\left((3+\lambda)^2 + 9\omega^2\tau_D^2\right)^2}, \tag{17}$$

where we have introduced the dimensionless parameter γ as

$$\gamma = \frac{kT\Delta\alpha}{\mu^2}, \tag{18}$$

which measures the relative contribution of the induced dipole compared to the permanent one. Thus, in the context of the rotational diffusion model, the dynamic Kerr effect response of an ensemble of interacting polar and polarizable molecules can be evaluated from the simple analytic equations, Eqs. (15)–(17).

Finally, if interactions may be neglected, $\lambda \to 0$, we have

$$C(\omega) = \frac{\gamma}{90} + \frac{1}{30\left(1 + \omega^2\tau_D^2\right)}, \tag{19}$$

$$\alpha_2'^{(2)}(\omega) = \frac{\gamma}{10\left(9 + 4\omega^2\tau_D^2\right)} + \frac{\left(3 - 2\omega^2\tau_D^2\right)}{10\left(1 + \omega^2\tau_D^2\right)\left(9 + 4\omega^2\tau_D^2\right)}, \tag{20}$$

$$\alpha_2''^{(2)}(\omega) = \frac{\gamma\omega\tau_D}{15\left(9+4\omega^2\tau_D^2\right)} + \frac{\omega\tau_D}{2\left(1+\omega^2\tau_D^2\right)\left(9+4\omega^2\tau_D^2\right)}, \tag{21}$$

while in the limit where interactions and induced moments are neglected, $\lambda \to 0$ and $\gamma \to 0$, we recover the results of Benoit[7] and Coffey and Paranjape,[8] viz.,

$$C(\omega) = \frac{1}{30\left(1+\omega^2\tau_D^2\right)}, \tag{22}$$

$$\alpha_2'^{(2)}(\omega) = \frac{\left(3-2\omega^2\tau_D^2\right)}{10\left(1+\omega^2\tau_D^2\right)\left(9+4\omega^2\tau_D^2\right)}, \tag{23}$$

$$\alpha_2''^{(2)}(\omega) = \frac{\omega\tau_D}{2\left(1+\omega^2\tau_D^2\right)\left(9+4\omega^2\tau_D^2\right)}. \tag{24}$$

Equations (15)–(17) are the main results of the present work.

III. RESULTS AND DISCUSSION

We have obtained the birefringence function $K(t) \sim \langle P_2(\cos\vartheta)\rangle(t)$ for an assembly of interacting polar and anisotropically polarizable molecules, Eqs. (14)–(17) via the mean field approximation. As far as the DC component of the birefringence function $C(\omega)$ is concerned, we see, by comparing our results and those of Benoit[7] and Coffey and Paranjape,[8] that only the characteristic time scale $\tau_1 = 3\tau_D/(3+\lambda)$ of the first-rank relaxation function is affected by interactions, while the spectrum of the birefringence function $C(\omega)$ itself remains the same (Lorentzian). This phenomenon is a consequence of neglecting the various interaction terms involving the induced dipole moments. As such terms are generally expected to be weak, this feature is of interest in interpreting related experimental data. By contrast, the situation is rather different for the AC part of the birefringence function, as is exemplified in Fig. 1, where the quantity $B(\omega)$ defined by

$$B(\omega) = \left[\left(\alpha_2'^{(2)}(\omega)\right)^2 + \left(\alpha_2''^{(2)}(\omega)\right)^2\right]^{1/2} \tag{25}$$

is plotted as a function of $\omega\tau_D$ for various values of the interaction parameter λ and for various values of γ. Clearly, the *nonmonotonic* behavior exhibited by $B(\omega)$ for moderate to large values of λ for vanishing induced dipole moments, i.e., $\gamma \to 0$ [see Figs. 1(a) and 1(b)], is a signature of the presence of intermolecular interactions. This result is analogous to that found in Ref. 15, where in contrast to the Coffey-Paranjape result $\lambda \to 0$ such behavior is absent. Now, as illustrated in Figs. 1(c) and 1(d), a consistent increase in the induced dipole moment will mask this non-monotonic behavior at large λ, as the leading term in the right-hand side of Eqs. (16) and (17) is no longer the second one (its amplitude varies as λ^{-2} at large λ) instead it is the first one involving *induced* dipoles. The high-frequency behavior of $B(\omega)$ is typically

$$B(\omega) \propto \frac{a_1}{\omega} + \frac{a_2}{\omega^2},$$

where a_1 and a_2 are coefficients such that $a_1 \propto \gamma$ and a_2 is independent of γ and is of *purely polar* origin. For the sake of illustration, the effect of induced dipoles is exaggerated on Fig. 2.

Now, one of the most noteworthy features of the dielectric relaxation of disordered materials and complex liquids such as glass-forming liquids, liquid crystals, and amorphous polymers is the failure of the rotational diffusion model to adequately describe the low-frequency spectra of their linear dielectric susceptibilities which are characterized by a broad distribution of relaxation times.[26] The relaxation processes in such complex systems are characterized by the temporally nonlocal behavior arising from the energetic disorder, which produces obstacles or traps, simultaneously delaying the motion of the particle and producing memory effects. A distribution of microscopic relaxation times may be included by averaging Eqs. (15)–(17) over an appropriate distribution such as Cole-Cole, Cole-Davidson, or Havriliak-Negami ones,[24] constituting an empirical way to proceed. One may therefore ask whether this effect may be included in the

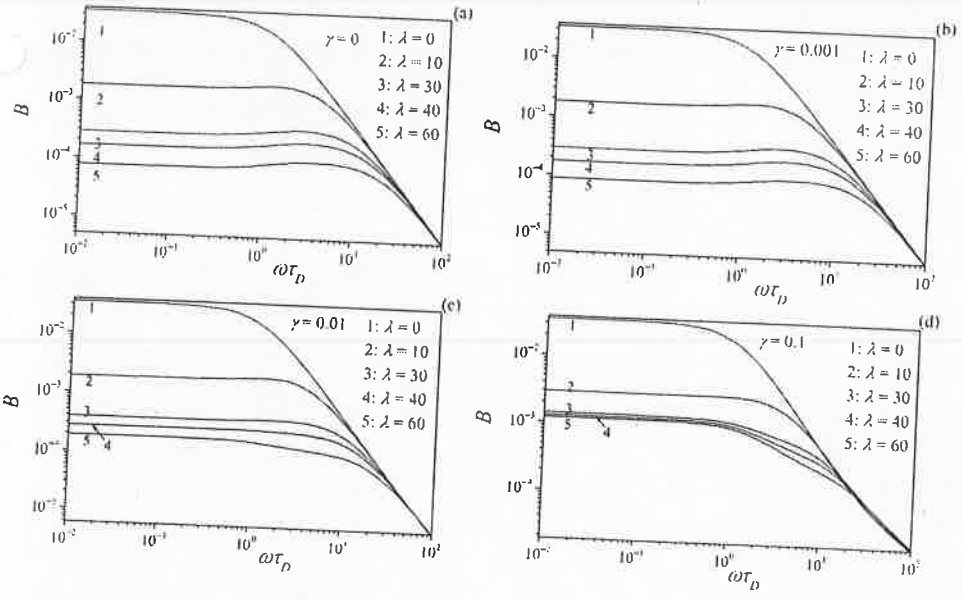

FIG. 1. $B(\omega)$ [Eq. (25)] vs $\omega\tau_D$ for various interaction parameters λ and $\gamma = 0$ (i.e., purely permanent moments) (a), $\gamma = 0.001$ (b), $\gamma = 0.01$ (c), and $\gamma = 0.1$ (d).

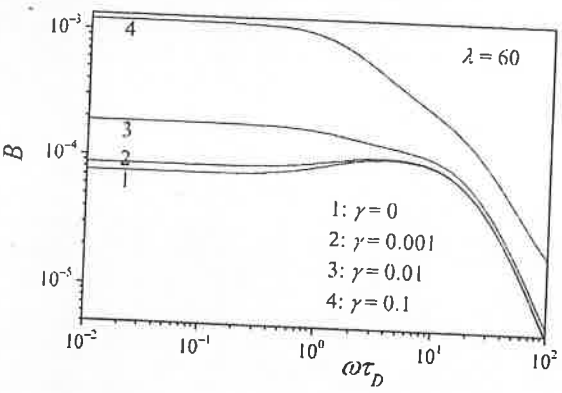

FIG. 2. $B(\omega)$ [Eq. (25)] vs $\omega\tau_D$ for various values of γ and $\lambda = 60$.

present theory by means of the fractional rotational diffusion equation, in the spirit of the approach of Coffey *et al.*[27] This would constitute another possibility to introduce the dielectric friction effect (and therefore indirectly dynamical effects) due to the molecular field, ultimately leading to the broadening and asymmetry of the nonlinear response spectra. However, the rigorous way to include such effects in the present theory is not clear because the basic diffusion Eq. (1) from which we have derived our results is *nonlinear*, while the standard Smoluchowski equation used in Ref. 27 is linear.

We may also notice that our calculation is a mean-field one because the orientational pair probability density factorizes in a product of single-body densities so that the orientational pair distribution function is unity throughout the present calculation (Smoluchowski-Vlasov approximation). This means that our formulas can be compared with experiment only qualitatively, save maybe for λ of order unity and below this value. For a quantitative comparison with experiment involving large λ values, orientational correlations are a necessary ingredient to account for in the calculation, which becomes then far more involved than the present one. Therefore, our conjectures remain only qualitative. Still, they suggest that intermolecular interactions can be studied by electro-optical methods such as the dynamic Kerr effect in AC fields or electric dichroism.

To conclude, we have described an analytical calculation of the AC stationary dynamic Kerr-effect response of *interacting* polar and polarizable molecules in the mean field approximation so effectively generalizing the existing results for noninteracting dipoles in AC driving fields. Our method can be also used in analogous nonlinear response problems involving time-dependent stimuli in high ac external fields. In particular, it can be applied with small modifications to magnetic birefringence relaxation of ferrofluids (colloidal suspensions of magnetic nanoparticles) because the magnetization dynamics of uniaxial magnetic nanoparticles are governed by equations very similar to Eq. (1).[28] Finally, the range of applicability of the rotational diffusion model in the mean field potential is restricted to the low-frequency range ($\omega\tau_I << 1$, where $\tau_I = I/\varsigma$ is the angular velocity relaxation time, I is the moment of inertia of a molecule, and ς is the rotational friction coefficient) because it does not include inertial effects. A consistent treatment of these effects must be carried out using the Fokker-Planck equation for the probability density function in configuration-angular velocity space.

ACKNOWLEDGMENTS

S. D. Deshmukh is grateful to program EUPHRATES for financial support of this work. We acknowledge stimulating discussions with Dr. F. Ladieu regarding several aspects on dielectric relaxation in polar fluids.

APPENDIX: RELATION BETWEEN THE DYNAMIC KERR EFFECT AND THE LINEAR DIELECTRIC RESPONSE

Here we discuss the relation between the DC dynamic Kerr effect and the linear dielectric response in the context of the present dynamical mean field model. First, we remark that the linear steady-state dielectric response to a pure AC field is given by

$$P^{(1)}(t) = \rho_0 \mu f_1^{(1)}(t) = \rho_0 \mu \xi_0 \left[\alpha_1'^{(1)}(\omega)\cos\omega t + \alpha_1''^{(1)}(\omega)\sin\omega t\right],$$

where $P_1^{(1)}(t)$ is the linear part of the polarization, $f_1^{(1)}(t)$ is given by Eq. (13), and $\alpha_1'^{(1)}(\omega)$ and $\alpha_1''^{(1)}(\omega)$ are the in-phase and out of phase components of the linear polarization and are [cf. Eq. (13)]

$$\alpha_1'^{(1)}(\omega) = \frac{(3+\lambda)}{(3+\lambda)^2 + 9\omega^2\tau_D^2}, \alpha_1''^{(1)}(\omega) = \frac{3\omega\tau_D}{(3+\lambda)^2 + 9\omega^2\tau_D^2}. \quad \text{(A1)}$$

These components are related via the Kramers-Kronig relations,[28] viz.

$$\alpha_1'^{(1)}(\omega) = \frac{2}{\pi}\int_0^\infty \frac{x\alpha_1''^{(1)}(x)\,dx}{x^2-\omega^2}, \alpha_1''^{(1)}(\omega) = -\frac{2}{\pi}\int_0^\infty \frac{\omega\alpha_1'^{(1)}(x)\,dx}{x^2-\omega^2}. \quad \text{(A2)}$$

Now, by examining the DC Kerr effect component $C(\omega)$ given by Eq. (15), we may remark that

$$C(\omega) = \frac{\gamma}{90} + \frac{3}{10(3+\lambda)}\alpha_1'^{(1)}(\omega). \quad \text{(A3)}$$

This means that both $C(\omega)$ and $\alpha_1'^{(1)}(\omega)$ contain the same *dynamical* information. Thus, in the context of the dynamical mean field model, the linear dielectric out-of-phase component may be deduced from Eqs. (A2) and (A3). Of course, this situation might differ if the dynamical orientational correlations are accounted for in the calculation, which then becomes much more involved.

[1]J. R. McConnell, *Rotational Brownian Motion and Dielectric Theory* (Academic, London, 1980).
[2]H. Watanabe and A. Morita, Adv. Chem. Phys. **56**, 255 (1984).
[3]E. Fredericq and C. Houssier, *Electric Dichroism and Electric Birefringence* (Clarendon, Oxford, 1973).

[4]Yu. L. Raikher and M. I. Shliomis, Adv. Chem. Phys. **87**, 595 (1994).
[5]W. T. Coffey, D. S. F. Crothers, Yu. P. Kalmykov, and P.-M. Déjardin, Phys. Rev. E **71**, 062102 (2005).
[6]N. Wei, P.-M. Déjardin, Yu. P. Kalmykov, and W. T. Coffey, Phys. Rev. E **93**, 042208 (2016).
[7]H. Benoit, Ann. Phys. **12**(6), 561 (1951).
[8]W. T. Coffey and B. V. Paranjape, Proc. R. Ir. Acad., Sect. A **78**, 17 (1978).
[9]H. Block and E. F. Hayes, Trans. Faraday Soc. **66**, 2512 (1970).
[10]R. Zwanzig, J. Chem. Phys. **38**, 2766 (1963).
[11]H.-X. Zhou and B. Bagchi, J. Chem. Phys. **97**, 3610 (1992).
[12]B. J. Berne, J. Chem. Phys. **62**, 1154 (1975).
[13]M. Warchol and W. E. Vaughan, J. Chem. Phys. **71**, 502 (1979).
[14]P.-M. Déjardin, J. Appl. Phys. **110**, 113921 (2011).
[15]P.-M. Déjardin and F. Ladieu, J. Chem. Phys. **140**, 034506 (2014).
[16]P. Madden and D. Kivelson, Adv. Chem. Phys. **56**, 467 (1984).
[17]T. W. Nee and R. Zwanzig, J. Chem. Phys. **52**, 6353 (1970).
[18]B. K. P. Scaife, *Principles of Dielectrics* (Clarendon, Oxford, 1989).
[19]C. J. F. Böttcher, *Theory of Electric Polarization* (Elsevier, Amsterdam, 1973), Vol. 1.
[20]W. T. Coffey and B. K. P. Scaife, Proc. R. Ir. Acad., Sect. A **76**, 195 (1976).
[21]J. H. Van Vleck, J. Chem. Phys. **5**, 556 (1937).
[22]M. S. Beevers, J. Crossley, D. C. Garrington, and G. Williams, J. Chem. Soc., Faraday Trans. 2 **72**, 1482 (1976).
[23]V. Rosato and G. Williams, J. Chem. Soc., Faraday Trans. 2 **77**, 1767 (1981).
[24]H. A. Kramers, Physica **7**, 284 (1940).
[25]F. Ladieu, D. L'Hôte, and C. Brun, Phys. Rev. B **85**, 184207 (2012).
[26]C. J. F. Böttcher and P. Bordewijk, *Theory of Electric Polarization* (Elsevier, Amsterdam, 1978), Vol. 2.
[27]W. T. Coffey, Yu. P. Kalmykov, and S. V. Titov, Adv. Chem. Phys. **133B**, 285 (2006).
[28]W. T. Coffey and Y. P. Kalmykov, *The Langevin Equation*, 4th ed. (World Scientific, Singapore, 2017).

Colloids and Surfaces A 537 (2018) 303–309

Contents lists available at ScienceDirect

Colloids and Surfaces A

journal homepage: www.elsevier.com/locate/colsurfa

Research Paper

EDA modified PANI/SWNTs nanocomposite for determination of Ni(II) metal ions

Megha A. Deshmukh[a,b], Harshada K. Patil[a,b], Gajanan A. Bodkhe[a,b], Mikito Yasuzawa[c], Pankaj Koinkar[d], Arunas Ramanavicius[e,f], Sadhna Pandey[g], Mahendra D. Shirsat[a,b,*]

[a] Department of Physics, Dr. Babasaheb Ambedkar Marathwada University, Aurangabad, MS 431 004, India
[b] RUSA-Center for Advanced Sensor and Technology, Dr. Babasaheb Ambedkar Marathwada University, Aurangabad, MS 431 004, India
[c] Department of Applied Chemistry, Tokushima University, Tokushima 770-8506, Japan
[d] Department of Optical Science, Tokushima University, Tokushima 770-8506, Japan
[e] Vilnius University, Faculty of Chemistry, Department of Physical Chemistry, Naugarduko St. 24, LT-03225 Vilnius, Lithuania
[f] State Research Institute Center for Physical Sciences and Technology, Laboratory of Bio Nano Technology, Savanoriu Ave. 231, LT-01108 Vilnius, Lithuania
[g] Department of Law, Dr. Babasaheb Ambedkar Marathwada University, Aurangabad, MS 431004, India

GRAPHICAL ABSTRACT

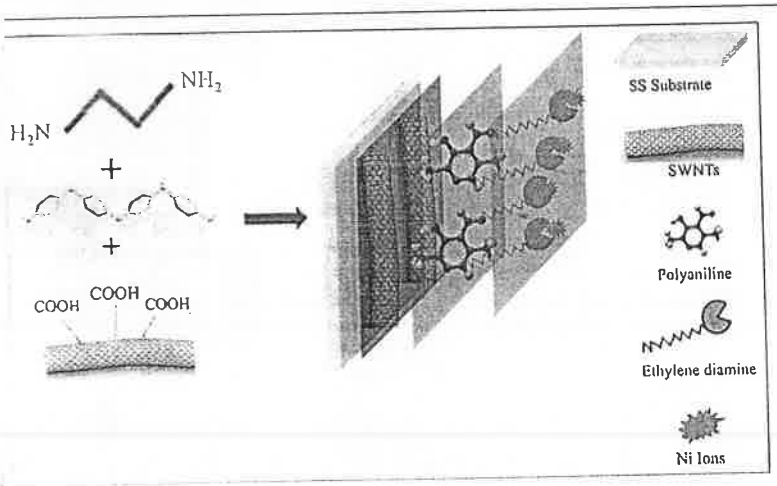

Scheme 1 Representation of the formation of ethyleendiamine modified PANI/SWNTs nanocompsite based electrochemical sensor for sensitive and selective detection of Ni(II) ions.

The formation of EDA modified PANI/SWNTs nanocomposite for detection of Ni(II) ions is shown in Scheme 1. The PANI/SWNTs nanocomposite structure was deposited on stainless steel (SS)-304 substrate through electrochemical route. Further the nanocomposite was modified with ethylenediamine via dip coating technique at room temperature.

ARTICLE INFO

Keywords:
Ethylenediamine
DPV
Nanocomposite sensor
Electrochemical analysis
Simultaneous detection

ABSTRACT

Present communication deals with demonstration of a simple and facile approach towards electrochemical synthesis of single walled carbon nanotubes (SWNTs) and polyaniline (PANI) nanocomposite by electrochemical method and its application for the detection of Ni(II) metal ion from aqueous media in presence of ethylenediamine (EDA) chelating ligand. The modification of PANI/SWNTs nanocomposite with EDA was done through simple dip coating technique at room temperature. Polyaniline (PANI) and single walled carbon nanotubes (SWNTs) nanocomposite considered as a sensing backbone. EDA served the purpose of selective detection of Ni

* Corresponding author at: RUSA-Center for Advanced Sensor Technology, Department of Physics, Dr. Babasaheb Ambedkar Marathwada University, Aurangabad, MS 431 004, India.
E-mail address: mdshirsat.phy@bamu.ac.in (M.D. Shirsat).

http://dx.doi.org/10.1016/j.colsurfa.2017.10.026
Received 9 September 2017; Received in revised form 4 October 2017; Accepted 8 October 2017
Available online 09 October 2017
0927-7757/

Nickel ion

(II) metal ion from aqueous media due to its ring-like structure. Ethylenediamine functionalized PANI/SWNTs nanocomposite (EDA-PANI/SWNTs) properties are evident from Electrochemical, Fourier transform infrared spectrometer (FTIR), Raman Spectroscopy, X-ray diffraction (XRD) and Atomic force microscope (AFM) analysis. Differential Pulse Voltammetry (DPV) technique was applied for the electrochemical analysis of Ni(II) ion. All recorded observations revealed that EDA modified PANI/SWNTs nanocomposite is suitable for the detection of Ni(II) ion.

1. Introduction

Contemporary carbon nanotubes (CNTs) and organic conducting polymer (OCP) based nanocomposite materials are grasping the attention of research communities due to their nanometer-sized structures and excellent properties [1–5]. High surface to volume ratio of nanocomposite materials is a key factor for the catalytic activities. The nanocomposite materials also show outstanding magnetic, optical, electronic, chemical, and electrochemical properties. In fact CNTs were first time discovered in 1991 by Sumio Ijjima [6]. CNTs have excellent electrical properties as well as large surface area compared to other carbon based materials. CNTs shows improved mechanical properties like high tensile strength, flexibility due to its Sp^2 bonded carbon structure [7,8]. CNTs are insoluble in water due to their polar nature [9] and likely advisable for the most of the analytical applications. CNTs can be functionalized covalently and non-covalently with a variety of materials to form the modified and composite electrode materials for plenty of applications with improved properties [10,11]. The extraordinary properties of CNTs, such as ease of functionalization ability, high surface to volume ratio, unique thermal, chemical, electrical and mechanical properties make them most preferred material for plenty of applications [12,13].

OCPs have enormous chemical, mechanical, optical and electrical properties and these properties as a result OCPs have been explored for various applications [14–17]. OCPs are enough flexible to make reversible changes in conductivity, color, mass and volume via doping, owing to their unique conjugated p-electron system [18–20]. Thus, OCPs Viz., polyaniline (PANI), polypyrrole (PPy), and polythiophene (PTh) are having great deal of interest and widely applicable for electrode materials due to their high conductivity, high pseudo capacitance, low cost, environmental stability, and ease of synthesis [21–24]. However, in spite of all these suitable properties, OCPs have some limitations in their use due to the considerable volume change during the repeated intercalation and depletion of ions during charge and discharge process which is responsible for the largely decrease in mechanical stability of OCPs [25]. In this context, CNTs are promising materials to incorporate with OCPs to facilitate and improve the performance of OCPs for various applications due to their high surface area and high mechanical strength, electrical conductivity and chemical stability [26,27].

In 1994 Ajayan et al., has first reported the great advantage of the composite structure of CNTs-OCPs utilizing their individual countless profitable properties [28,29]. The combination of CNTs and OCPs based composite materials can achieve improved synergistic effect which means to achieve an efficient electro catalysis [30,31].

Thus, CNTs-OCPs composite structure have a wide range of applications in quite large number of fields such as, biomedical [32], orthopedic implants [33], treatment of periodontal diseases in dentistry [34], VOC sensors [35] etc.

In this regard, herein we have synthesized a single walled carbon nanotubes (SWNTs) – polyaniline (PANI) composite with ethylenediamine (EDA) as modifier chelating ligand for the detection of Ni(II) ion from the aqueous phase. PANI can interact with SWNTs via π-π stacking which corresponds to non-covalent bonding. In the composite formation, SWNTs will act as a backbone of the structure surrounded by PANI molecules. EDA molecules will bind to the surface of PANI molecules and can firmly attach through π-π interaction which gives the ethylenediamine modified PANI-SWNTs nanocomposite for the selective and sensitive detection of Ni (II) ions.

2. Experimental

2.1. Materials and reagents

Aniline of reagent grade was purchased from Sigma Aldrich (Bangalore, India); Dodecyl benzene sulphonic acid sodium salt (DBSA) was procured from Kemphasol (Bombay, India) and it was used as surfactant and organic solvent to form fine suspension of SWNTs. H_2SO_4 of HPLC grade acquired from Rankem (Bombay, India), SWNTs functionalized with carboxyl groups (-COOH) were purchased fro Nanoshel LLC. Ethylenediamine (EDA) was procured from Fisher Scientific, 1-ethyl-3(3 (dimethyl amino) propyl)-Carbodiimide (EDC) was procured from Sigma Aldrich (Bangalore, India). Phosphate buffer with pH 7, and other chemicals were reagent grade quality and they were used as received. Stainless Steel (SS type 304, 0.5 mm thick and area 1 × 1 cm^2) purchased from MTI (Korea). Metal salt of $Ni(NO)_3$ was procured from Fisher Scientific. All processes were performed in aqueous media and the preparation of the aqueous solutions were carried out using ultra-pure quality of water.

2.2. Synthesis of PANI/SWNTs nanocomposite

PANI/SWNTs nanocomposite was synthesized by an electrochemical method using cyclic voltammetry technique. Briefly, 0.25 M of aniline monomer and 0.5 M of H_2SO_4 were added in distilled water (100 ml). It was 12% wt. of SWNTs in distilled water with respect to the concentration of aniline monomer. DBSA was added as a surfactant in the SWNTs + DI (Deionized water) solution to make fine suspension of the SWNTs with the ratio of 10:1 (DBSA:SWNTs) sonicated for 6 h Resulting suspension of SWNTs was added slowly to the aniline + H_2SO_4 solution, stirred for 20 min at room temperature using magnetic stirrer. The final electrolyte of aniline + H_2SO_4 + SWNTs w utilized for the electrochemical synthesis of PANI/SWNTs nanocomposite.

Cyclic Voltammetry technique was used for electrochemical synthesis of PANI/SWNTs nanocomposite. SS substrate was used as a working electrode, Platinum plate as a counter electrode and Ag/AgCl as a reference electrode for synthesis of composite. The potential was scanned between 0.1–1.0 V for 20 cycles at the scan rate of 0.1 V/s. The composite formation on working electrode was observed by dark green colored coating with respect to the applied potential and cycles. The deposited dark green colored film was washed thoroughly with DI water to remove the excess monomer on a substrate surface and further dried at room temperature.

2.3. Preparation of EDA modified PANI/SWNTs nanocomposite

For the preparation of chelating ligand solution, 0.1 M of EDC (crosslinking agent) was added to the 0.01 M of EDA in 100 ml of distilled water and stirred for 20 min at room temperature. The electrochemically prepared PANI/SWNTs nanocomposite thin film was dipped in the EDA solution for 5 h at room temperature. After completion of dipping period the EDA modified nanocomposite film was rinsed through distilled water to remove the loosely bound EDA particles on

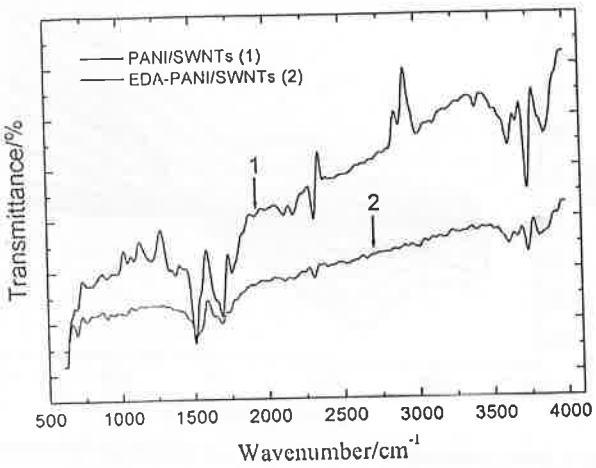

Fig. 3. FTIR spectra of PANI/SWNTs (Line 1)and EDA-PANI/SWNTs (Line 2) nanocomposite.

aniline monomer and SWNTs as well as modification of nanocomposite by EDA revealed from FTIR analysis. The PANI/SWNTs spectrum shows the basic bands for appearance of PANI molecules such as band at 1433 cm^{-1} and 1510 cm^{-1} for the benzoid and quinod band formation which are the characteristics bands of the PANI. The band near about 1220 cm^{-1} reveals emeraldine form and confirms the conducting nature of PANI. A broad peak at 3404 cm^{-1} is due to the N–H stretching vibration of the aromatic amine. The bands at 1219 cm^{-1} and 795 cm^{-1} can be assigned for the C–N stretching of the secondary aromatic amine and C–H aromatic out of-plane bending vibration, respectively. The band at 1048 cm^{-1} attributed for the presence of CNTs. All these band are getting supressed in the EDA modified PANI/SWNTs composite structure. These results confirms that EDA molecules are getting accumulated on the PANI/SWNTs nanocomposite and dominating the characteristic bands of PANI/SWNTs nanocomposite. In EDA modified spectra the vibrational modes attributed for the free amine groups such as NH_2 scissoring at 1523 cm^{-1}, C–N stretching at 1098 cm^{-1}, 1033 cm^{-1} and NH wagging at 942 cm^{-1}. The band at 1686 cm^{-1} assigned for EDA is the NH_2 (Primary amine).

3.4. XRD analysis of PANI/SWNTs and EDA modified PANI/SWNTs nanocomposite

The structural analysis of PANI/SWNTs nanocomposite before and after modification with EDA was carried out using X-Ray Diffraction (XRD) pattern (BRUKER D8 Advance). Fig. 4 shows the diffraction

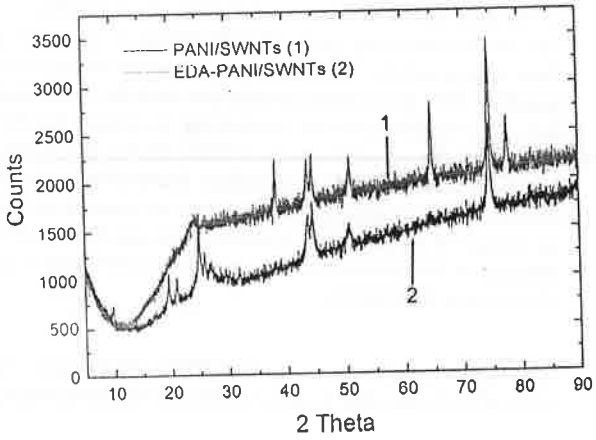

Fig. 4. XRD of (Black line) PANI/SWNTs and (Line 1) EDA modified PANI/SWNTs (Line 2) nanocomposite. (For interpretation of the references to colour in this figure legend, the reader is referred to the web version of this article.)

pattern of the nanocomposite before and after modification. The diffraction pattern for PANI/SWNTs and EDA-PANI/SWNTs nanocomposite was recorded broad scattering at 2θ values within 10°–90°. For PANI/SWNTs nanocomposite characteristic peaks for SWNTs appeared at $2\theta = \sim 25°$ and lower intensity peak at $2\theta = \sim 43°$, as reported earlier [37]. For PANI typical peaks observed at $2\theta = \sim 20°$ corresponding to (020) crystal plane of PANI. The presence of peak at 25°accredited to the periodicity parallel to the polymer chain reveling the semi crystalline nature of material [38]. Thus, the observed characteristic peaks of PANI and SWNTs, indicating successful synthesis of PANI/SWNTs nanocomposite. In comparison of PANI/SWNTs nanocomposite and EDA modified nanocomposite, it has been observed that there is an increase in intensity of peaks after modification. After modification of PANI/SWNTs nanocomposite with EDA, the characteristic peaks observed in PANI/SWNTs nanocomposite structure seems to be suppressed due to accumulation of EDA molecules on nanocomposite structure. This result shows homogeneous coating of EDA onto the PANI/SWNTs nanocomposite surface indicating that PANI/SWNTs nanocomposite has successfully modified with EDA and is in well agreement with the results obtained from AFM.

3.5. Raman analysis of PANI/SWNTs and EDA modified PANI/SWNTs nanocomposite

Fig. 5 shows the Raman spectra of PANI/SWNTs and EDA modified PANI/SWNTs nanocomposite. In PANI/SWNTs nanocomposite, the presence of a broad G band at 1592 cm^{-1} and D band at 1351 cm^{-1} was observed. In the EDA modified nanocomposite, the D and G bands slightly shifted towards the left side due to the modification of nanocomposite structure. The presence of D induces the presence of amorphous disordered carbon structure of CNTs [39] and G band for the stretching band of C–C bond respectively [40]. The band at 1309 cm^{-1} in the nanocomposite corresponds to the $C–N^+$ stretching, but in the EDA modified nanocomposite the same band is shifting to lower wavenumber at 1198 cm^{-1} with less intensity. The shifting could be attributed to electrostatic interaction between the $C–N^+$ species of PANI and $-COO$ species of SWNTs in nanocomposite [41]. But in EDA modified nanocomposite the intensity of same band is decreased, this might be due to dominating effect of EDA molecules over PANI/SWNTs electrostatic interaction. The enhancement of delocalization degree of $C–N^+$ segment shows increased intensity due to the presence of SWNTs [42] however, in modified nanocomposite intensity is decreases due to accumulation of EDA molecules on the nanocomposite. This clearly indicates that EDA ions got accumulated on the surface of nanocomposite.

3.6. Morphological analysis of PANI/SWNTs and EDA modified PANI/SWNTs nanocomposite

The AFM images for the PANI/SWNTs nanocomposite confirm rod like shape. The rod like structure formation of AFM reveals that SWNTs got coated by polyaniline. In this nanocomposite formation, CNTs are revealing as a backbone of the structure and polyaniline as the coating layer. The rod like shapes are clearly visible and separated from each other. In the structure of PANI/SWNTs nanocomposite, the presence of SWNTs is more evident. However in EDA modified PANI/SWNTs structure, SWNTs are hardly visible due to accumulation of EDA molecules on nanocomposite structure. In nanocomposite (PANI/SWNTs) longer and thicker structures appears compared to EDA modified PANI/SWNTs. From these observations it can be concluded that SWNTs got coated with PANI molecules and in modified nanocomposite whole composite structure is covered with EDA molecules. Fig. 6c shows histogram recorded from AFM scan images of PANI/SWNTs and EDA-PANI/SWNTs nanocomposite. Roughness of EDA modified PANI/SWNTs is more compared to unmodified nanocomposite. More roughness would be better to adsorb the analyte on surface area.

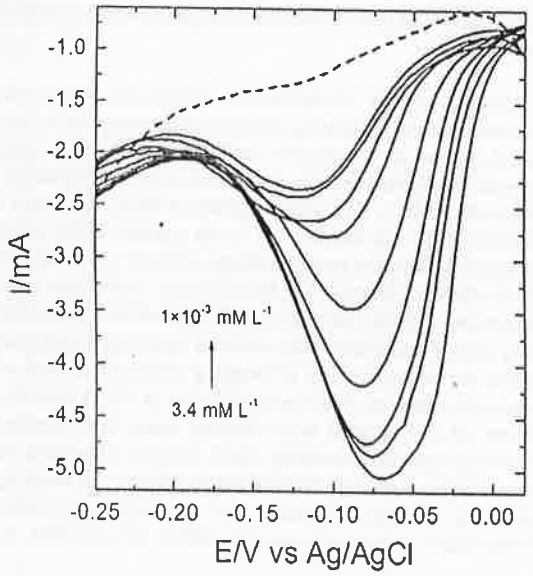

Fig. 7. Differential pulse voltammograms of SS electrodes modified by EDA modified PANI/SWNTs layer recorded in acetic acid buffer solution (pH 2.1), containing differential Ni(II) ion concentrations: 3.4 mM, 0.3 mM, 6×10^{-2} mM, 3×10^{-2} mM, 6×10^{-3} mM, 3×10^{-3} mM, 2×10^{-3} mM, 1×10^{-3} mM L^{-1}, respectively.

SWNTs after this step recorded from −0.25 to 0.01 V in a separate blank solution of 0.5 M H_2SO_4. DPV exhibit anodic peak in between 0.0 to −0.1 V versus Ag/AgCl corresponding to the reduced of Ni(II) ions at EDA modified PANI/SWNTs surface. Overlapped differential pulse voltammogram curve shows response towards Ni(II) at EDA modified PANI/SWNTs layer modified SS-electrode for various concentrations (Fig. 7). However, no current peak was recorded after incubation of EDA modified PANI/SWNTs layer in blank solution (it is represented as reference curve (Dotted line)). The lower detection limit observed for Ni(II) ion is 1×10^{-3} mM L^{-1}.

Very few reports are available on the DPV based electrochemical detection of Ni(II) ion. As listed in Table 1, spectroscopic and colorimetric techniques are widely used analytical techniques for accurate detection of metal ions. However, spectroscopic techniques are accountable for time consuming sample pre-treatment procedures and usage of sophisticated instrumentation [43]. In colorimetric techniques comparable colors from interfering substances can produce errors in results [44]. However, the reported ethylenediamine modified nanocomposite for detection of Ni(II) ion by electrochemical technique shows sensitive and selective response towards the Ni(II) ions.

Selectivity of the sensor is one of the most important characteristic of the any sensor. Ethylenediamine is a bidentate ligand that is able to form two coordinative bonds with a metal atom through the lone pair of

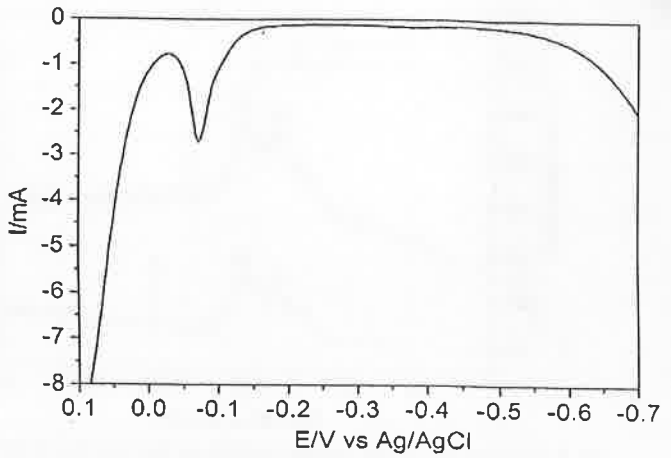

Fig. 8. DPV curve recorded in acetic acid buffer solution (pH 2.1) for selective detection of Ni(II) ions in the presence of Pb(II), Cd(II), Cu(II), Hg(II) and Co(II) ions.

electrons on both nitrogens [55]. Compared to alkaline earth and alkali metal cations the transition metal cations mostly shows strong affinity towards ethylenediamine [56]. In case of selective detection of Ni ions with ethylenediamine ligand, a single molecule of ethylenediamine is able to form two bonds to a transition metal ion, such as Ni(II). The bond formation can take place between the metal ion and the nitrogen atoms of ethylenediamine. The Ni(II) ion can form six such bonds; hence, a maximum of three ethylenediamine molecules can be attached to one Ni(II) ion [57]. However, EDA modified PANI/SWNTs nanocomposite shows selective response towards Ni(II) ion.

Fig. 8 shows DPV of Ni (II) ions in acetic acid buffer solution (pH 2.1) as the supporting electrolyte medium using EDA modified PANI/SWNTs. The EDA modified PANI/SWNTs electrode was immersed in a solution containing 2 of Pb(II), Cd(II), Hg(II), Co(II), Cu(II) ions for 10 min. The DPV plot shows the clear anodic peaks only for Ni(II). EDA showed selectivity towards only Ni(II) ions.

4. Conclusions

Electrochemical synthesis and modification of PANI/SWNTs nanocomposite with EDA chelating ligand was successfully carried out. An electrochemical, spectroscopic and morphological characterization of PANI/SWNTs and EDA modified PANI/SWNTs confirms the information of chemical bonding and morphological differences between PANI/SWNTs nanocomposite and EDA modified PANI/SWNTs nanocomposite. The EDA modified PANI/SWNTs nanocomposite was used for detection of Ni(II) ion. The EDA modified PANI/SWNTs exhibit excellent sensing behaviour with lower detection limit of 1×10^{-3} mM L^{-1}.

Table 1
Overview of some sensing materials used in electrochemical and optical sensors for the determinatio of Ni(II) ions.

Sr. No.	Sensing Material	Detection limit	Sensing technique	Ref.
01	A thio carboxylic acid derivative:2-aminocyclopent-1-ene-1-carbodithioic acid (ligand)	0.5 ppm	Colorimetric	[45]
02	Modified miswak fibers by NaOH (AT-Miswak-F).	2.1 ng mL^{-1}	Infrared spectroscopy	[46]
03	Imine ligands, (E)-N1-(2-hydroxy-5 nitrobenzylidene) isonicotinoylhydrazone and 2-(4-fluoro benzylideneamino) benzenethiol	0.89 ng and 0.82 ng L^{-1}	Spectrophotometric	[47]
04	Triangular silver nanoprisms (AgNPRs) stabilized with glutathione (GSH)	50 nM	Colorimetric	[48]
05	boron-doped diamond electrode	26.1 μM	Electrochemical	[49]
06	Hydrazone Derivative Immobilized on the Triacetyl Cellulose Membrane	1.00×10^{-10} mol L^{-1}	Spectrophotometric	[50]
07	1 Leached Ag Nanoparticles	10 nM	Colorimetric	[51]
08	2 Quinoline	5.0×10^{-6} M	Colorimetric	[52]
09	3 Tetra(*m*-aminophenyl)porphyrin (Tm-APP)	3 ng L^{-1}	Reversed-phase high-performance liquid chromatography (RP-HPLC)	[53]
10	Nafion-graphene dimethylglyoxime modified glassy carbon electrode	1.5 μg L^{-1}	Adsorptive Stripping Voltammetry	[54]

Acknowledgements

This work was supported by the Department of Science and Technology (DST)-SERB, New Delhi, India (Project No. SB/EMEQ-042/2013); Inter University Accelerator Center (IUAC), New Delhi, India (UFR No. 55305); Rashtriaya Uchhatar Shiksha Abhiyan, Govt. of Maharashtra, India (RUSA/order/R & I/2016-17); UGC-SAP, New Delhi, India (F.530/16/DRS-I/2016(SAP-II)).

References

[1] L. Yang-Ling, Effective approaches for the preparation of organo-modified multi-walled carbon nanotubes and the corresponding MWCNT/polymer nanocomposites, Polym. J. 48 (2016) 345–358.

[2] V. Chaitra, P. Eugenia, I. Amor, A. Marc, J. James, T. Alexandre, T. Ghazal, K. Adriana, R. Daria, S. Jose-Ramon, D. Elfis, R. Leo, P. Abhay, J. Manus, Polyhydroxyalkanoate/carbon nanotube nanocomposites: flexible electrically conducting elastomers for neural applications, Nanomedicine 11 (2016) 2547–2563.

[3] C. Serena, P. Elisa, P. Andrea, R. Giacomo, Nanocomposites based on thermoplastic polymers and functional nanofiller for sensor applications, Materials 8 (2015) 3377–3427.

[4] P. Harshada, D. Megha, G. Sumedh, B. Gajanan, K. Asokan, Y. Mikito, K. Pankaj, S. Mahendra, Influence of oxygen ions irradiation on polyaniline/single walled carbon nanotubes nanocomposite, Radiat. Phys. Chem. 130 (2017) 47–51.

[5] D. Kunal, G. Prasanta, R. Arti, M. Ashok, S. Mahendra, Fe nanoparticles tailored poly(N-methyl pyrrole) nanowires matrix: a CHEMFET study in perspective of discrimination among electron donating analytes, J. Phys. D: Appl. Phys. 48 (2015) 1–8.

[6] S. Iijima, T. Ichihashi, Single-shell carbon nanotubes of 1-nm diameter, Nature 363 (1993) 603–605.

[7] J. Yang, X. Li, C. Luo, G. Ma, Changes of structure and electrical conductivity of multi-walled carbon nanotubes film caused by 3 MeV proton irradiation, Appl. Surf. Sci. 325 (2015) 235–241.

[8] P. Martins Jr., C. Alcântara, R. Resende, A. Ferreira, Carbon nanotubes directions and perspectives in oral regenerative medicine, J. Dent. Res. 92 (2013) 575–583.

[9] W. Chen, L. Duan, D. Zhu, Adsorption of polar and nonpolar organic chemicals to carbon nanotubes, Environ. Sci. Technol. 41 (2007) 8295–8300.

[10] S. Vashist, D. Zheng, K. Al-Rubeaan, J. Luong, F. Sheu, Advances in carbon nanotube based electrochemical sensors for bioanalytical applications, Biotechnol. Adv. 29 (2011) 169–188.

[11] P. Gregorio, Nunes, M. Tomasina, L. Poma, Covalent grafting of carbon nanotubes in PA-6 matrix to improve compatibility, Compos. Part B 46 (2013) 61–68.

[12] Y. Luo, X. Wei, D. Cao, R. Bai, F. Xu, Y. Chen, Polystyrene-block-poly (tert-butyl methacrylate)/multiwall carbon nanotube ternary conducting polymer nanocomposites based on compatibilizers: preparation, characterization and vapor sensing applications, Mater. Des. 87 (2015) 149–156.

[13] A. Díez-Pascual, M. Naffakh, C. Marco, M. Gómez-Fatou, G. Ellis, Multiscale fiber-reinforced thermoplastic composites incorporating carbon nanotubes: a review, Curr. Opin. Solid State Mater. Sci. 18 (2014) 62–80.

[14] H. Park, T. Kim, J. Huh, M. Kang, J. Lee, H. Yoon, Anisotropic growth control of polyaniline nanostructures and their morphology-dependent electrochemical characteristics, ACS Nano 6 (2012) 7624–7633.

[15] M. Chang, T. Kim, H. Park, M. Kang, F. Reichmanis, H. Yoon, Imparting chemical stability to nanoparticulate silver via a conjugated polymer casing approach, ACS Appl. Mater. Interfaces 4 (2012) 4357–4365.

[16] T. Zheng, W. Wang, G. Zhu, A. Wang, Enhanced selectivity for heavy metals using polyaniline-modified hydrogel, Ind. Eng. Chem. Res. 52 (2013) 4957–4961.

[17] D. Kwon, S. Park, H. Park, T. Kim, M. Kang, J. Jang, H. Yoon, Kinetically controlled formation of multidimensional poly(3,4-ethylenedioxythiophene) nanostructures in vapor-deposition polymerization, Chem. Mater. 24 (2012) 4088–4092.

[18] H. Yoon, Current trends in sensors based on conducting polymer nanomaterials, Nanomaterials 3 (2013) 524–549.

[19] S. Park, O. Kwon, J. Lee, J. Jang, H. Yoon, Conducting polymer-based nanohybrids transducers: a potential route to high sensitivity and selectivity sensors, Sensors 14 (2014) 3604–3630.

[20] H. Yoon, J. Jang, Conducting-polymer nanomaterials for high-performance sensor applications: issues and challenges, Adv. Funct. Mater. 19 (2009) 1567–1576.

[21] A. Burke, R & D considerations for the performance and application of electrochemical capacitors, Electrochim. Acta 53 (2007) 1083–1091.

[22] K. Frackowiak, V. Khomenko, K. Jurewicz, K. Lota, F. Béguin, Supercapacitors based on conducting polymers/nanotubes composites, J. Power Sources 153 (2006) 413–418.

[23] T. Girija, M. Sangaranarayanan, Analysis of polyaniline-based nickel electrodes for electrochemical supercapacitors, J. Power Sources 156 (2006) 705–711.

[24] J. Kim, K. Kim, K. Kim, Fabrication and electrochemical properties of carbon nanotube/polypyrrole composite film electrodes with controlled pore size, J. Power Sources 176 (2008) 396–402.

[25] C. Peng, S. Zhang, D. Jewell, G. Chen, Carbon nanotube and conducting polymer composites for supercapacitors, Prog. Nat. Sci. 18 (2008) 777–788.

[26] J. Issi, L. Langer, J. Heremans, C. Olk, Electronic properties of carbon nanotubes: experimental results, Carbon 33 (1995) 941–948.

[27] R. Ma, Study of electrochemical capacitors utilizing carbon nanotube electrodes, J. Power Sources 84 (1999) 126–129.

[28] M. Ates, Review study of (bio) sensor systems based on conducting polymers, Mater. Sci. Eng. C 33 (2013) 1853–1859.

[29] F. Al-Oqla, S. Sapuan, T. Anwer, M. Jawaid, M. Hoque, Natural fiber reinforced conductive polymer composites as functional materials: a review, Synth. Met. 206 (2015) 42–54.

[30] T. Lien, T. Lam, V. An, T. Hoang, D. Quang, D. Khieu, T. Tsukahara, Y. Lee, K. Kim, Multi-wall carbon nanotubes (MWCNTs)-doped polypyrrole DNA biosensor for label-free detection of genetically modified organisms by QCM and EIS, Talanta 80 (2010) 1164–1169.

[31] C. Peng, J. Jin, G. Chen, Comparative study on electrochemical co-deposition and capacitance of composite films of conducting polymers and carbon nanotubes, Electrochim. Acta 53 (2007) 525–537.

[32] D. Zhang, M. Kandadai, J. Cech, S. Roth, S. Curran, Poly(L-lactide) (PLLA)/multiwalled carbon nanotubes (MWCNT) composite: characterization and biocompatibility evaluation, J. Phys. Chem. B 110 (2006) 12910–12915.

[33] R. Spear, R. Cameron, Carbon nanotubes for orthopaedic implants, Int. J. Mater. Form. 1 (2008) 127–133.

[34] J. Yang, Z. Yao, C. Tang, B. Darvell, H. Zhang, L. Pan, J. Liu, Z. Chen, Growth of apatite on chitosan-multiwall carbon nanotube composite membranes, Appl. Surf. Sci. 255 (2009) 8551–8555.

[35] Y. Luo, X. Wei, D. Cao, R. Bai, F. Xu, Y. Chen, Polystyrene-block-poly (tert-butyl methacrylate)/multiwall carbon nanotube ternary conducting polymer nanocomposites based on compatibilizers: preparation, characterization and vapor sensing applications, Mater. Des. 87 (2015) 149–156.

[36] M.F. De Riccardis, M. Virginia, New method to obtain hybrid conducting nanocomposites based on polyaniline and carbon nanotubes, Energia Ambiente e innovazione 6 (2011) 86–95.

[37] O. Zhou, R. Fleming, D. Murphy, C. Chen, R. Haddon, A. Ramirez, S. Glarum, Defects in carbon nanostructures, Science 263 (1994) 1744–1747.

[38] A. Tursun, U. Aminam, R. Jamal, R. Adalet, Solid-state synthesis of polyaniline/single-walled carbon nanotubes: a comparative study with polyaniline/multi-walled carbon nanotubes, Materials 5 (2012) 1219–1231.

[39] M. Dresselhaus, G. Dresselhaus, R. Saito, A. Jorio, Raman spectroscopy of carbon nanotubes, Physics Rep. 409 (2005) 47–99.

[40] M. Cochet, G. Louarn, S. Quillard, J. Buisson, S. Lefrant, Theoretical and experimental vibrational study of emeraldine in salt form. Part II, J. Raman Spectrosc. 31 (2000) 1041–1049.

[41] X. Yan, Z. Han, Y. Yang, B. Tay, Fabrication of carbon nanotube-polyaniline composites via electrostatic adsorption in aqueous colloids, J. Phys. Chem. C 111 (2007) 4125–4131.

[42] I. Šeděnková, M. Trchová, J. Stejskal, Thermal degradation of polyaniline films prepared in solutions of strong and weak acids and in water – FTIR and Raman spectroscopic studies, Polym. Degrad. Stab. 93 (2008) 2147–2157.

[43] Modi Wang, Ka-Ho Leung, Sheng Lin, Daniel Shiu-Hin Chan, Daniel W.J. Kwong, Chung-Hang Leung, Dik-Lung Ma, A colorimetric chemosensor for Cu2+ ion detection based on an iridium(III) complex, Sci. Rep. 4 (2014) 1–7.

[44] A. Wallace Hayes, Principles and Methods of Toxicology, fifth edition, CRC Press, Taylor and Francis group, 2008.

[45] Y.L.N. Murthy, B. Govindh, B.S. Diwakar, K. Nagalakshmi, R. Singh, A simple inexpensive detection method of nickel in water using optical sensor, Int. J. Chem. Technol. Res. 3 (2011) 1285–1291.

[46] E.A. Moawed, M.A. Elghamry, M.A. Elagrasy, M.F. ElShahat, Determination of iron, cobalt and nickel ions from aqueous media using the alkali modified miswak, J. Assoc. Arab Univ. Basic Appl. Sci. 23 (2017) 43–51.

[47] B.N. Kumar, S. Kanchi, M.I. Sabela, K. Bisetty, N.V.V. Jyothi, Spectrophotometric determination of nickel (II) in waters and soils: novel chelating agents and their biological applications supported by DFT method, Karbala Int. J. Mod. Sci. 2 (2016) 239–250.

[48] N. Chen, Y. Zhang, H. Liu, H. Ruan, C. Dong, Z. Shen, A. Wu, A supersensitive probe for rapid colorimetric detection of nickel ion based on a sensing mechanism of anti-etching, Sustain. Chem. Eng. 4 (2016) 6509–6516.

[49] S. Neodo, M. Nie, J.A. Wharton, K.R. Stokes, Nickel-ion detection on a boron-doped diamond electrode in acidic media, Electrochim. Acta 88 (2013) 18–724.

[50] K. Alizadeh, N.A. Rad, A new optical sensor for selective monitoring of nickel ion based on a hydrazone derivative immobilized on the triacetyl cellulose membrane, J. Anal. Bioanal. Technol. 7 (2016) 1–6.

[51] W. Tianxiang, M. Zhanfang, Colorimetric detection of cobalt or nickel ions based on the change of the catalytic performance of leached Ag nanoparticles, J. Nanosci. Nanotechnol. 17 (2017) 4297–4303.

[52] X. Liu, Q. Lin, T. Wei, Y. Zhang, A highly selective colorimetric chemosensor for detection of nickel ions in aqueous solution, New J. Chem. 38 (2014) 1418–1423.

[53] Q. Hu, G. Yang, Y. Zhao, J. Yin, Determination of copper nickel, cobalt, silver, lead, cadmium, and mercury ions in water by solid-phase extraction and the RP-HPLC with UV–vis detection, Anal. Bioanal. Chem. 375 (2003) 831–835.

[54] K. Pokpas, N. Jahed, P.G. Baker, E.I. Iwuoha, Complexation-based detection of Nickel(II) at a graphene-chelate probe in the presence of cobalt and zinc by adsorptive stripping voltammetry, Sensors 17 (2017) 1711–1722.

[55] J.K. Beattle, conformational analysis of Tristethylenediamine) Complexes, Acc. Chem. Res. 4 (1971) 253–259.

[56] C. De Stefano, C. Foti, S. Sammartano, Interaction of polyamines with Mg^{2+} and Ca^{2+}, J. Chem. Eng. Data 44 (1999) 744–749.

[57] C. Watkins, G. Vigee, Ethylenediamine complexes of copper (II) and nickel (II) in solutions of dimethyl sulfoxide, J. Phys. Chem. 80 (1976) 83–88.

Acknowledgements

This work was supported by the Department of Science and Technology (DST)-SERB, New Delhi, India (Project No. SB/EMEQ-042/2013); Inter University Accelerator Center (IUAC), New Delhi, India (UFR No. 55305); Rashtriaya Uchhatar Shiksha Abhiyan, Govt. of Maharashtra, India (RUSA/order/R & I/2016-17); UGC-SAP, New Delhi, India (F.530/16/DRS-I/2016(SAP-II)).

References

[1] E. Ying-Ling, Effective approaches for the preparation of organo-modified multi-walled carbon nanotubes and the corresponding MWCNT/polymer nanocomposites, Polym. J. 48 (2016) 571–588.
[2] V. Catalina, P. Eugenia, L. Artur, A. Marc, J. James, T. Alexandre, T. Ghazal, K. Adriana, B. Ilana, S. Jose-Ramon, D. Ellis, R. Leo, P. Abhay, J. Manus, Polyhydroxyalkanoate/carbon nanotube nanocomposites: flexible electrically conducting elastomers for neural applications, Nanomedicine 11 (2016) 2547–2563.
[3] C. Serena, P. Elisa, P. Andrea, R. Giacomo, Nanocomposites based on thermoplastic polymers and functional nanofiller for sensor applications, Materials 8 (2015) 3377–3427.
[4] P. Harshada, D. Megha, G. Sumedh, B. Gajanan, K. Asokan, Y. Mikito, K. Pankaj, S. Mahendra, Influence of oxygen ions irradiation on polyaniline/single walled carbon nanotubes nanocomposite, Radiat. Phys. Chem. 130 (2017) 47–51.
[5] D. Kumar, C. Prasanta, R. Ajit, M. Ashok, S. Mahendra, Fe nanoparticles tailored poly(N-methyl pyrrole) nanowires matrix: a CHEMFET study in perspective of discrimination among electron donating analytes, J. Phys. D: Appl. Phys. 48 (2015) 1–8.
[6] S. Iijima, T. Ichihashi, Single-shell carbon nanotubes of 1-nm diameter, Nature 363 (1993) 603–605.
[7] J. Yang, X. Li, C. Liu, G. Ma, Changes of structure and electrical conductivity of multi-walled carbon nanotubes film caused by 3 MeV proton irradiation, Appl. Surf. Sci. 325 (2015) 235–241.
[8] P. Martins Jr., C. Alcântara, R. Resende, A. Ferreira, Carbon nanotubes directions and perspectives in oral regenerative medicine, J. Dent. Res. 92 (2013) 575–583.
[9] W. Chen, L. Duan, D. Zhu, Adsorption of polar and nonpolar organic chemicals to carbon nanotubes, Environ. Sci. Technol. 41 (2007) 8295–8300.
[10] S. Vashist, D. Zheng, K. Al-Rubeaan, J. Luong, F. Sheu, Advances in carbon nanotube based electrochemical sensors for bioanalytical applications, Biotechnol. Adv. 29 (2011) 169–188.
[11] P. Singha, J. Xavier, N. Tamanna, L. Pama, Covalent grafting of carbon nanotubes to PEEK to improve compatibility, Compos. Part B 46 (2013) 61–68.
[12] Y. Luo, X. Wei, D. Cao, R. Bai, F. Xu, Y. Chen, Polystyrene-block-poly (tert-butyl methacrylate)/multiwall carbon nanotube ternary conducting polymer nanocomposites based on compatibilizers: preparation, characterization and vapor sensing applications, Mater. Des. 87 (2015) 149–156.
[13] A. Díez-Pascual, M. Naffakh, C. Marco, M. Gómez-Fatou, G. Ellis, Multiscale fiber-reinforced thermoplastic composites incorporating carbon nanotubes: a review, Curr. Opin. Solid State Mater. Sci. 18 (2014) 62–80.
[14] H. Park, T. Kim, J. Huh, M. Kang, J. Lee, H. Yoon, Anisotropic growth control of polyaniline nanostructures and their morphology-dependent electrochemical characteristics, ACS Nano 6 (2012) 7624–7633.
[15] M. Chang, T. Kim, H. Park, M. Kang, E. Reichmanis, H. Yoon, Imparting chemical stability to nanostructured silver via a conjugated polymer casing approach, ACS Appl. Mater. Interfaces 4 (2012) 4357–4365.
[16] Y. Zheng, W. Wang, G. Zhu, A. Wang, Enhanced selectivity for heavy metals using polyaniline-modified hydrogel, Ind. Eng. Chem. Res. 52 (2013) 4957–4961.
[17] O. Kwon, S. Park, H. Park, T. Kim, M. Kang, J. Jang, H. Yoon, Kinetically controlled formation of multidimensional poly(3,4-ethylenedioxythiophene) nanostructures in vapor-deposition polymerization, Chem. Mater. 24 (2012) 4088–4092.
[18] H. Yoon, Current trends in sensors based on conducting polymer nanomaterials, Nanomaterials 3 (2013) 524–549.
[19] S. Park, O. Kwon, J. Lee, J. Jang, H. Yoon, Conducting polymer-based nanohybrids transducers: a potential route to high sensitivity and selectivity sensors, Sensors 14 (2014) 3604–3630.
[20] H. Yoon, J. Jang, Conducting-polymer nanomaterials for high-performance sensor applications: issues and challenges, Adv. Funct. Mater. 19 (2009) 1567–1576.
[21] V. Khomenko, E. Frackowiak, B. Béguin, Exploration of the parameters for the performance and application of electrochemical capacitors, Electrochim. Acta 53 (2007) 1083–1091.
[22] E. Frackowiak, V. Khomenko, K. Jurewicz, K. Lota, F. Béguin, Supercapacitors based on conducting polymers/nanotubes composites, J. Power Sources 153 (2006) 413–418.
[23] T. Girija, M. Sangaranarayanan, Analysis of polyaniline-based nickel electrodes for electrochemical supercapacitors, J. Power Sources 156 (2006) 705–711.
[24] J. Kim, K. Kim, K. Kim, Fabrication and electrochemical properties of carbon nanotube/polypyrrole composite film electrodes with controlled pore size, J. Power Sources 176 (2008) 396–402.
[25] C. Peng, S. Zhang, D. Jewell, G. Chen, Carbon nanotube and conducting polymer composites for supercapacitors, Prog. Nat. Sci. 18 (2008) 777–788.
[26] J. Issi, J. Langer, J. Heremans, C. Olk, Electronic properties of carbon nanotubes: experimental results, Carbon 33 (1995) 941–948.
[27] R. Ma, Study of electrochemical capacitors utilizing carbon nanotube electrodes, J. Power Sources 84 (1999) 126–129.
[28] M. Ates, Review study of (bio) sensor systems based on conducting polymers, Mater. Sci. Eng. C 33 (2013) 1853–1859.
[29] F. Al-Oqla, S. Sapuan, T. Anwer, M. Jawaid, M. Hoque, Natural fiber reinforced conductive polymer composites as functional materials: a review, Synth. Met. 206 (2015) 42–54.
[30] T. Lien, T. Lam, V. An, T. Hoang, D. Quang, D. Khieu, T. Tsukahara, Y. Lee, K. Kim, Multi-wall carbon nanotubes (MWCNTs)-doped polypyrrole DNA biosensor for label-free detection of genetically modified organisms by QCM and EIS, Talanta 80 (2010) 1164–1169.
[31] C. Peng, J. Jin, G. Chen, Comparative study on electrochemical co-deposition and capacitance of composite films of conducting polymers and carbon nanotubes, Electrochim. Acta 53 (2007) 525–537.
[32] D. Zhang, M. Kandadai, J. Cech, S. Roth, S. Curran, Poly(L-lactide) (PLLA)/multiwalled carbon nanotubes (MWCNT) composite: characterization and biocompatibility evaluation, J. Phys. Chem. B 110 (2006) 12910–12915.
[33] R. Spear, R. Cameron, Carbon nanotubes for orthopaedic implants, Int. J. Mater. Form. 1 (2008) 127–133.
[34] J. Yang, Z. Yao, C. Tang, B. Darvell, H. Zhang, L. Pan, J. Liu, Z. Chen, Growth of apatite on chitosan-multiwall carbon nanotube composite membranes, Appl. Surf. Sci. 255 (2009) 8551–8555.
[35] Y. Luo, X. Wei, D. Cao, R. Bai, F. Xu, Y. Chen, Polystyrene-block-poly (tert-butyl methacrylate)/multiwall carbon nanotube ternary conducting polymer nanocomposites based on compatibilizers: preparation, characterization and vapor sensing applications, Mater. Des. 87 (2015) 149–156.
[36] M.F. De Riccardis, M. Virginia, New method to obtain hybrid conducting nanocomposites based on polyaniline and carbon nanotubes, Energia Ambiente e innovazione 6 (2011) 86–95.
[37] O. Zhou, R. Fleming, D. Murphy, C. Chen, R. Haddon, A. Ramirez, S. Glarum, Defects in carbon nanostructures, Science 263 (1994) 1744–1747.
[38] A. Tursun, U. Aminam, R. Jamal, R. Adalet, Solid-state synthesis of polyaniline/single-walled carbon nanotubes: a comparative study with polyaniline/multi-walled carbon nanotubes, Materials 5 (2012) 1219–1231.
[39] M. Dresselhaus, G. Dresselhaus, R. Saito, A. Jorio, Raman spectroscopy of carbon nanotubes, Physics Rep. 409 (2005) 47–99.
[40] M. Cochet, G. Louarn, S. Quillard, J. Buisson, S. Lefrant, Theoretical and experimental vibrational study of emeraldine in salt form. Part II, J. Raman Spectrosc. 31 (2000) 1041–1049.
[41] X. Yun, Z. Han, Y. Yang, B. Tay, Fabrication of carbon nanotube-polyaniline composites via electrostatic adsorption in aqueous colloids, J. Phys. Chem. C 111 (2007) 4125–4131.
[42] I. Šeděnková, M. Trchová, J. Stejskal, Thermal degradation of polyaniline films prepared in solutions of strong and weak acids and in water—FTIR and Raman spectroscopic studies, Polym. Degrad. Stab. 93 (2008) 2147–2157.
[43] Modi Wang, Ka-Ho Leung, Sheng Lin, Daniel Shiu-Hin Chan, Daniel W.J. Kwong, Chung-Hang Leung, Dik-Lung Ma, A colorimetric chemosensor for Cu2 + ion detection based on an iridium(III) complex, Sci. Rep. 4 (2014) 1–7.
[44] A. Wallace Hayes, Principles and Methods of Toxicology, fifth edition, CRC Press, Taylor and Francis group, 2008.
[45] Y.L.N. Murthy, B. Govindh, B.S. Diwakar, K. Nagalakshmi, R. Singh, A simple inexpensive detection method of nickel in water using optical sensor, Int. J. Chem. Technol. Res. 3 (2011) 1285–1291.
[46] E.A. Moawed, M.A. Elghamry, M.A. Elagrasy, M.F. ElShahat, Determination of iron, cobalt and nickel ions from aqueous media using the alkali modified miswak, J. Assoc. Arab Univ. Basic Appl. Sci. 23 (2017) 43–51.
[47] B.N. Kumar, S. Kanchi, M.I. Sabela, K. Bisetty, N.V.V. Jyothi, Spectrophotometric determination of nickel (II) in waters and soils: novel chelating agents and their biological applications supported by DFT method, Karbala Int. J. Mod. Sci. 2 (2016) 239–250.
[48] N. Chen, Y. Zhang, H. Liu, H. Ruan, C. Dong, Z. Shen, A. Wu, A supersensitive probe for rapid colorimetric detection of nickel ion based on a sensing mechanism of anti-etching, Sustain. Chem. Eng. 4 (2016) 6509–6516.
[49] S. Neodo, M. Nie, J.A. Wharton, K.R. Stokes, Nickel-ion detection on a boron-doped diamond electrode in acidic media, Electrochim. Acta 88 (2013) 18–724.
[50] K. Alizadeh, N.A. Rad, A new optical sensor for selective monitoring of nickel ion based on a hydrazone derivative immobilized on the triacetyl cellulose membrane, J. Anal. Bioanal. Technol. 7 (2016) 1–6.
[51] W. Tianxiang, M. Zhanfang, Colorimetric detection of cobalt or nickel ions based on the change of the catalytic performance of leached Ag nanoparticles, J. Nanosci. Nanotechnol. 17 (2017) 4297–4303.
[52] X. Liu, Q. Lin, T. Wei, Y. Zhang, A highly selective colorimetric chemosensor for detection of nickel ions in aqueous solution, New J. Chem. 38 (2014) 1418–1423.
[53] Q. Hu, G. Yang, Y. Zhao, J. Yin, Determination of copper nickel, cobalt, silver, lead, cadmium, and mercury ions in water by solid-phase extraction and the RP-HPLC with UV–vis detection, Anal. Bioanal. Chem. 375 (2003) 831–835.
[54] K. Pokpas, N. Jahed, P.G. Baker, E.I. Iwuoha, Complexation-based detection of Nickel(II) at a graphene-chelate probe in the presence of cobalt and zinc by adsorptive stripping voltammetry, Sensors 17 (2017) 1711–1722.
[55] J.K. Beattle, conformational analysis of Tris(ethylenediamine) Complexes, Acc. Chem. Res. 4 (1971) 253–259.
[56] C. De Stefano, C. Foti, S. Sammartano, Interaction of polyamines with Mg^{2+} and Ca^{2+}, J. Chem. Eng. Data 44 (1999) 744–749.
[57] C. Watkins, G. Vigee, Ethylenediamine complexes of copper (II) and nickel (II) in solutions of dimethyl sulfoxide, J. Phys. Chem. 80 (1976) 83–88.